Nuclear Engineering and Technology 53 (2021) 4130–4136

Contents lists available at ScienceDirect

Nuclear Engineering and Technology

journal homepage: www.elsevier.com/locate/net

Original Article

Gadolinium- and lead-containing functional terpolymers for low energy X-ray protection

Yu-Juan Zhang [a], Xin-Tao Guo [b], Chun-Hong Wang [a, *], Xiang An Lu [c, **], De-Feng Wu [a], Ming Zhang [a]

[a] School of Chemistry and Chemical Engineering, Yangzhou University, Yangzhou, China
[b] Department of Materials Research, AVIC Manufacturing Technology Institute, Beijing, China
[c] Guangling College of Yangzhou University, Yangzhou, China

ARTICLE INFO

Article history:
Received 1 April 2021
Received in revised form
5 June 2021
Accepted 12 June 2021
Available online 25 June 2021

Keywords:
Metal-containing terpolymers
Mass attenuation coefficient
Parameter estimation
Ternary reactivity ratios

ABSTRACT

By polymerization of gadolinium methacrylate (Gd $(MAA)_3$), lead methacrylate ($Pb(MAA)_2$) and methyl methacrylate (MMA), Gd and Pb were chemically bonded into polymers. The X-ray shielding performance was evaluated by Monte Carlo simulation method, and the results showed that the more metal functional organic monomer, the better the shielding performance of terpolymers. When the X-ray energy is 65 keV, Gd $(MAA)_3$-containing polymers have better shielding performance than $Pb(MAA)_2$-containing polymers. Gd could compensate for the weak absorption region of Pb. Therefore, polymers containing both Gd and Pb enhanced shielding efficiency against X-ray in various low-energy ranges. For obtaining terpolymers with uniform monomer compositions, the relationship between the monomer composition of the terpolymers and the conversion level was optimized by calculating the reactivity ratios. The value of reactivity ratios of r (Gd $(MAA)_3$/$Pb(MAA)_2$), r ($Pb(MAA)_2$/Gd $(MAA)_3$), r (Gd $(MAA)_3$/MMA), r (MMA/Gd $(MAA)_3$), r ($Pb(MAA)_2$/MMA) and r (MMA/$Pb(MAA)_2$) was 0.483, 0.004, 0.338, 2.508, 0.255, 0.029. The terpolymers with uniform monomer composition could be obtained by controlling the monomer compositions or conversion levels. The results can provide new radiation protection materials and contribute to the improvement in nuclear safety.

1. Introduction

X-ray used in medical diagnosis and treatment has brought huge progress and convenience to the medical field [1,2]. However, it also brought potential harms to patients, medical staff or medical facility that exposed to the scattered rays and leaked radiation. Therefore, development of anti-X-ray materials is necessary. Radiation protection polymers have attracted more and more attention to the advantages of high performance, easy processing, light weight, and simple preparation method. etc. [2] Pb is commonly used to against low-energy X-ray through the photoelectric effect because of its larger atomic number [3], while Gd can compensate for the weak absorption region of Pb in the region of 40–88 keV [4,5]. Therefore, polymers containing both Gd and Pb are good low-energy X-ray shielding materials. Monte Carlo N Particle Transport Code (MCNP program) is commonly employed to access shielding properties of materials [6].

The preparation of metal-containing polymers by polymerization of organometallic salts and organic monomers is a very interesting method. Metal functional organic monomers, gadolinium methacrylate (Gd $(MAA)_3$) and lead methacrylate ($Pb(MAA)_2$) were synthesized and both could undergo free-radical co-polymerization with methyl methacrylate (MMA) [7,8]. In our previous work [9,10], the polymerization kinetics of self-polymerization and co-polymerization of Gd $(MAA)_3$ and $Pb(MAA)_2$ was studied, respectively. The results showed that metal functional organic monomers was more inclined to self-polymerize, which led to uneven dispersion of shielding elements in the material. However, the uniform distribution of shielding elements is an important factor of the stability and reliability of shielding materials, while the MCNP program is based on the ideal uniform distribution of the

* Corresponding author. School of Chemistry and Chemical Engineering, Yangzhou University, Yangzhou 225002, China.
** Corresponding author. Guangling College of Yangzhou University, Yangzhou 225002, China.
E-mail addresses: wangch@yzu.edu.cn (C.-H. Wang), 060178@yzu.edu.cn (X.A. Lu).

https://doi.org/10.1016/j.net.2021.06.021

elements. Compositions and sequence distributions of metal-organic copolymers were influenced by the monomer reactivity ratios, Therefore, it is necessary to estimate reliably the monomer reactivity ratios of this ternary system [11–14].

In this work, based on the photon shielding theory, the X-ray shielding performance of polymers containing different metal elements (including Gd-containing copolymers (poly (Gd $(MAA)_3$-MMA)), Pb-containing copolymers (poly $(Pb(MAA)_2$-MMA), and terpolymer containing both Gd and Pb (poly (Gd $(MAA)_3$-$Pb(MAA)_2$-MMA)) were assessed by the MCNP program. The kinetics of the systems, namely the ter-polymerization of the Gd $(MAA)_3$/$Pb(MAA)_2$/MMA in solution was studied. The relationship between terpolymer compositions and monomer feeding compositions, as well as conversion levels were obtained.

2. Materials and methods

2.1. Materials

Gadolinium methacrylate (Gd $(MAA)_3$) and lead methacrylate ($Pb(MAA)_2$) were made in the laboratory with their purity over 99% [9,10]. N,*N*-dimethylformamide (DMF, AR), methyl methacrylate (MMA, CP), methanol, ethanol, azobisiobutyronitrile (AIBN, CP) were obtained from Sinpharm Chemical Reagent Co. Ltd. China. Refining MMA by vacuum distillation, and AIBN was purified by recrystallization before use.

2.2. Ter-polymerization

Under nitrogen atmosphere, the ter-polymerization of Gd $(MAA)_3$, $Pb(MAA)_2$, and MMA with different feed compositions (as shown in Table 1) were carried out with 80 wt% DMF as the reaction medium. The reaction temperature was 70 °C. Based on total monomers, the initiator (AIBN) concentration was 5 wt%. Dissipating the heat generated during the polymerization process by stirring. The products were precipitated with methanol as a precipitant and then separated by filtration, washed with ethanol and dried in vacuum at 60 °C to a constant weight. The conversion level was calculated by weighing measurement.

2.3. Characterization

2.3.1. Monte Carlo simulation method

MCNP is a computer algorithm based on random sampling, and it is one of the most famous Monte Carlo simulation codes. The radiation source is defined by inputting the type, energy, geometric position and incident direction of incident particles, which are tracked by probability statistics. After a particle passing through the transmission plane, it stops tracking and starts to simulate the next particle until all the particles are simulated. The distribution of particle intensity and dose can be obtained by means of the data recorded by the detectors during the tracking process. The simulated geometric model was shown in Fig. 1. The source term was defined as a single-energy photon point source. The photon exits right along the *x*-axis, the energy of the radiation source was defined as from 30 keV to 100 keV. The calculated number of particles was 10^6. The detector was a cylinder with a diameter of 7 cm, with the incident surface of the detector as the detection surface. Counting with a F1 card to calculate the shielding rate of the material to X-ray. The shielding materials were metal-containing functional polymers with different metal content. Then using defining the thickness of composites as 4, 8, 12, 16, 20, 25, 30, and 40 mm. The elemental compositions of different copolymers were given in supporting information (Table S1, Table S2 and Table S3).

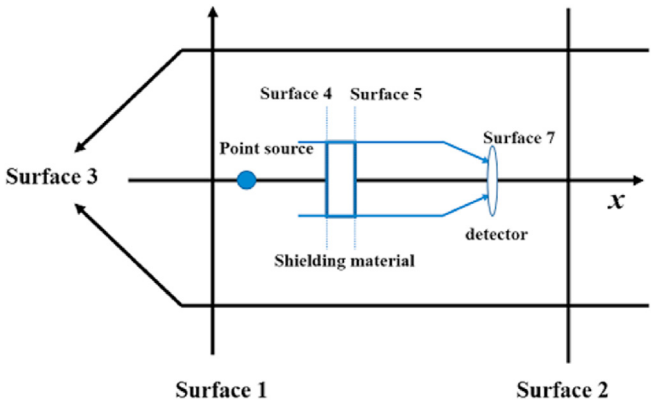

Fig. 1. Schematic diagram of Monte Carlo simulation method calculation of material radiation shielding performance.

The mass attenuation coefficient (MAC) is suitable for describing the attenuation of various radiation doses. The MAC is independent on the density and physical state of the material, which provides great convenience for practical applications. The attenuation of photons in the shielding material can be expressed by the Beer-Lambert law Eqn 1 [15]:

$$I = I_0\, e^{-\mu x} \tag{1}$$

$$\mu_x = \frac{\mu}{\rho} \tag{2}$$

where I_0 and I represent the initial (before the sample) and final (after the model) photon intensities, respectively; μ is linear

Table 1
Random conversion level data set.

Sample	Gd/$(MAA)_3$/$Pb(MAA)_2$/MMA (wt%)	*f* (mol%)	*F* (mol%)	Mass conversion (%)
1	5/30/65	1.64/10.72/87.64	4.06/41.54/54.40	14.89
2	5/60/35	2.57/33.77/63.66	3.32/61.35/35.33	43.53
3	5/70/25	2.71/41.46/55.83	2.67/58.37/38.96	34.50
4	5/80/15	3.24/56.69/40.07	2.21/71.17/26.62	15.28
5	5/90/5	4.03/79.35/16.62	1.69/61.99/36.32	8.86
6	20/25/55	7.30/9.98/82.72	15.36/47.33/37.31	10.45
7	20/55/25	10.92/32.83/56.25	12.18/67.84/19.98	17.62
8	40/15/45	16.54/6.78/76.68	32.02/21.92/46.06	18.34
9	40/45/5	26.50/32.57/40.93	20.22/49.35/30.42	23.79
10	60/10/30	30.84/5.62/63.54	46.07/12.14/41.79	22.96
11	60/30/10	44.78/24.47/30.75	34.94/32.78/32.28	26.58
12	80/5/15	54.32/3.71/41.97	52.25/4.35/43.30	30.60
13	80/15/5	68.38/14.01/17.61	43.01/12.66/44.33	41.79

attenuation coefficient and x is thickness of shielding material Eqn 2. The μ_m is the slope of the straight-line equation as the folumla (2), where ρ is the density of material [16,17].

2.3.2. X-ray diffractometer

D8 Advance X-ray diffractometer was used to obtain the X-ray diffractometer (XRD) pattern. The scanning angle (2θ) was from 5° to 60°, and the scanning speed was 2 °min^{-1}.

2.3.3. Fourier transform infrared spectroscopy

Attenuated total reflectance-Fourier transform infrared spectroscopy (ATR-FTIR) analysis of the synthesized sample was conducted using the Cary 610/670 micro-infrared spectrometer of American Varian Company. The scanning range was 4000–400 cm^{-1}, 4 cm^{-1} resolution and scanned 32 times continuously.

2.3.4. The composition analysis of terpolymers

The external beam particle-induced X-ray emission technique (PIXE) and ash method were employed to determine the composition analysis. Gd $(MAA)_3$, $Pb(MAA)_2$, and MMA polymerized to form cross-linked terpolymer. Therefore, it was difficult to quantitatively analyze the element content using general elemental analysis methods. PIXE technique is a method of qualitative and quantitative analysis of materials by bombarding a sample with a proton beam of a certain energy, and according to the energy and intensity of characteristic X-ray generated after the atoms in the sample are excited [18–21]. Grinding the sample into a fine powder with a mortar, and then dried under vacuum at 80 °C, for 6 h until completely dry. Sticking the sample on the double-sided tape and placing it upright on the sample holder. The elemental composition of the samples was determined by particle-induced X-ray emission (PIXE) at the 2 × 1.7 MV Tandetron accelerator of the Beijing Normal University. A 2.5 MeV proton beam was selected with a beam diameter of 6.8 mm and the beam current was controlled at 1–2 nA. Each PIXE spectra were collected by a computer-based multichannel analyzer with a data acquisition time of about 30 s. The Au–Si surface barrier detector was added to measure beam charge integration synchronously, by monitoring the proton's backscattered signal [22,23]. The element concentration is based on the collected PIXE spectral data, calculated with the GUPIXWIN software package, after inputting the determined geometric conditions and related experimental parameters [24–26].

Terpolymers were calcined in a muffle furnace at 800 °C, for 2 h to obtain the metal oxides (*i.e.* Gd_2O_3, PbO).

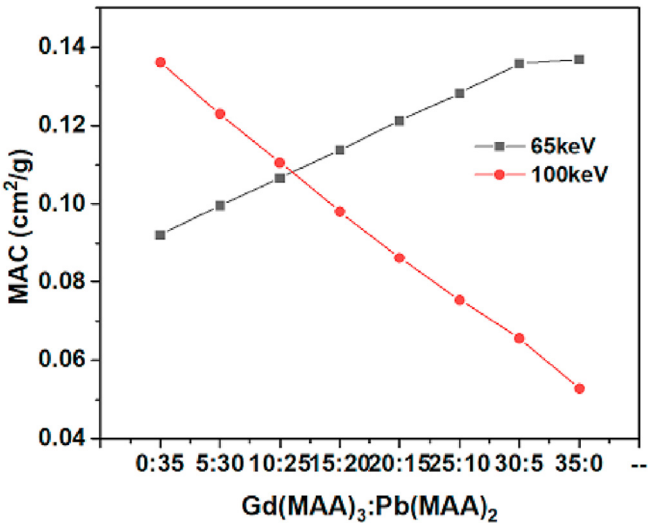

Fig. 3. The mass attenuation coefficient of poly (Gd $(MAA)_3$-$Pb(MAA)_2$-MMA).

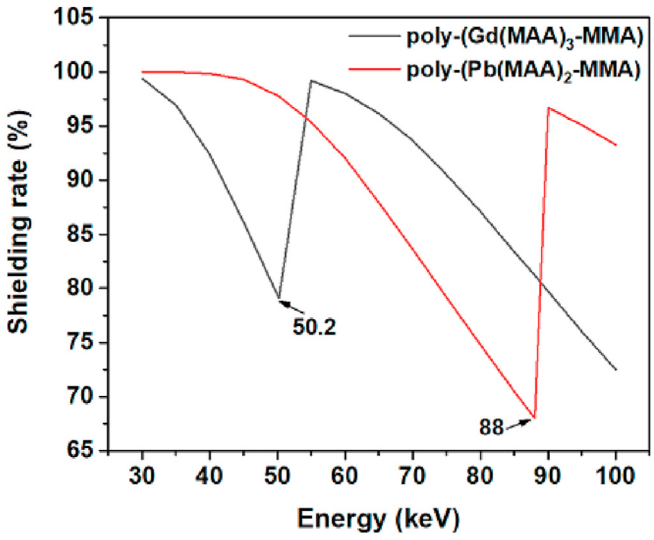

Fig. 4. Shielding rates of different functional polymer materials under different energies (The mass percentage of Gd $(MAA)_3$ and $Pb(MAA)_2$ in the copolymer was 30 wt %; the thickness of the copolymer was 20 cm).

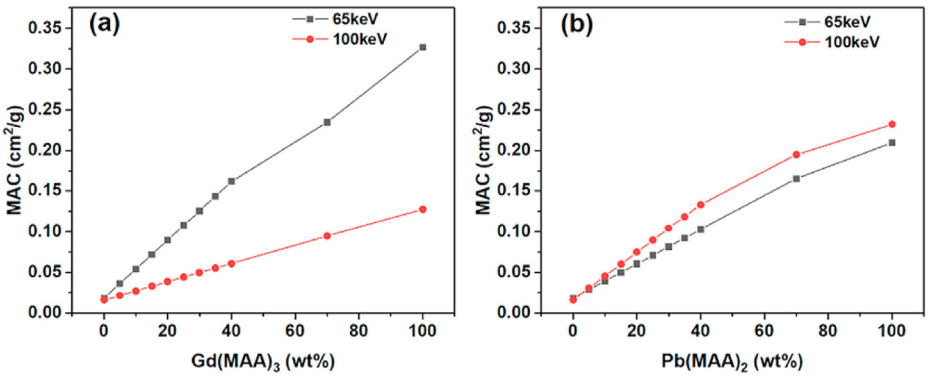

Fig. 2. The mass attenuation coefficient of the functional polymer.

2.4. Reactivity ratio estimation

It is correct and reliable to determine the ternary reactivity ratios by using the experimental data from the ter-polymerization directly to estimate reactivity ratios for each system [27,28]. Alfrey and Goldfinger (AG model) described the ternary polymerization reaction mathematically and derived the first composition equation of the ternary system [29]. Combined the AG model with direct numerical integration (DNI) to estimate the ternary reaction ratio rate can include more experimental information and avoid the limitation of data collection at low conversion levels. The error-in-variables model (EVM) is a parameter estimation method, which applied to linear and non-linear model that takes into account the problem of errors in all dependent and independent variables [30]. It is considered as the most statistically correct method for reactivity ratio estimation in multi-component polymerization systems, and it is very suitable for the AG model [31,32].

2.4.1. Cumulative ter-polymerization composition models

Kazemi et al. [33] modified the original form of the AG model (Eqn 3, 4 and 5). The instantaneous molar fraction of monomer i in the terpolymer chain in the model is expressed as F_i, and f_i represents the molar fraction of unreacted monomer i in the polymerizing mixture. formula (6) is the definition of monomer reaction rate (r_{ij}), and the rate constant of the reaction between the group i and the monomer is represented by k_{ij}.

$$r_{12}=\frac{k_{11}}{k_{12}}, r_{13}=\frac{k_{11}}{k_{13}}, r_{21}=\frac{k_{22}}{k_{21}}, r_{23}=\frac{k_{22}}{k_{23}}, r_{31}=\frac{k_{33}}{k_{31}}, r_{32}=\frac{k_{33}}{k_{32}} \tag{6}$$

To solve the problem of calculating the cumulative terpolymer composition at each conversion level, Kazemi et al. [34] had proposed the direct numerical integration approach (DNI) based on the famous Skeist equation which is given by formula (7), where $f_{i,0}$, and f_i are the mole fractions of monomer i in the initial and remaining mixture, respectively, ($\overline{F_i}$) is the cumulative terpolymer composition, and Xn represents the total molar conversion in the polymerization medium [35,36]. The molar fraction of unreacted monomer in the polymerization medium can be obtained by solving the differential terpolymer composition equation (formula (8)) of the terpolymer. The conversion level that can be directly measured through experiments is the weight conversion level (Xw), which needs to be converted to Xn by formula (9).

$$\overline{F_i}=\frac{f_{i,0}-f_i(1-X_n)}{X_n} \text{ or } i=1,2, \text{and } 3 \tag{7}$$

$$\frac{df_i}{dX_n}=\frac{f_i-F_i}{1-X_n} \text{ for } i=1,2 \text{ and } 3 \tag{8}$$

$$X_n=X_w\frac{Mw_if_{i,0}+Mw_jf_{j,0}+Mw_kf_{k,0}}{Mw_i\overline{F_i}+Mw_j\overline{F_j}}+Mw_k\overline{F_k} \tag{9}$$

$$F_1=\frac{f_1\left(\frac{f_1}{r_{21}r_{31}}+\frac{f_2}{r_{21}r_{32}}+\frac{f_3}{r_{31}r_{23}}\right)\left(f_1+\frac{f_2}{r_{12}}+\frac{f_3}{r_{13}}\right)}{f_1\left(\frac{f_1}{r_{21}r_{31}}+\frac{f_2}{r_{21}r_{32}}+\frac{f_3}{r_{31}r_{23}}\right)\left(f_1+\frac{f_2}{r_{12}}+\frac{f_3}{r_{13}}\right)+f_2\left(\frac{f_1}{r_{12}r_{31}}+\frac{f_2}{r_{21}r_{32}}+\frac{f_3}{r_{13}r_{32}}\right)\left(f_2+\frac{f_1}{r_{21}}+\frac{f_3}{r_{23}}\right)+f_3\left(\frac{f_1}{r_{13}r_{21}}+\frac{f_2}{r_{23}r_{12}}+\frac{f_3}{r_{13}r_{23}}\right)\left(f_3+\frac{f_1}{r_{31}}+\frac{f_2}{r_{32}}\right)} \tag{3}$$

$$F_2=\frac{f_2\left(\frac{f_1}{r_{12}r_{31}}+\frac{f_2}{r_{21}r_{32}}+\frac{f_3}{r_{13}r_{32}}\right)\left(f_2+\frac{f_1}{r_{21}}+\frac{f_3}{r_{23}}\right)}{f_1\left(\frac{f_1}{r_{21}r_{31}}+\frac{f_2}{r_{21}r_{32}}+\frac{f_3}{r_{31}r_{23}}\right)\left(f_1+\frac{f_2}{r_{12}}+\frac{f_3}{r_{13}}\right)+f_2\left(\frac{f_1}{r_{12}r_{31}}+\frac{f_2}{r_{21}r_{32}}+\frac{f_3}{r_{13}r_{32}}\right)\left(f_2+\frac{f_1}{r_{21}}+\frac{f_3}{r_{23}}\right)+f_3\left(\frac{f_1}{r_{13}r_{21}}+\frac{f_2}{r_{23}r_{12}}+\frac{f_3}{r_{13}r_{23}}\right)\left(f_3+\frac{f_1}{r_{31}}+\frac{f_2}{r_{32}}\right)} \tag{4}$$

$$F_3=\frac{f_3\left(\frac{f_1}{r_{13}r_{21}}+\frac{f_2}{r_{23}r_{12}}+\frac{f_3}{r_{13}r_{23}}\right)\left(f_3+\frac{f_1}{r_{31}}+\frac{f_2}{r_{32}}\right)}{f_1\left(\frac{f_1}{r_{21}r_{31}}+\frac{f_2}{r_{21}r_{32}}+\frac{f_3}{r_{31}r_{23}}\right)\left(f_1+\frac{f_2}{r_{12}}+\frac{f_3}{r_{13}}\right)+f_2\left(\frac{f_1}{r_{12}r_{31}}+\frac{f_2}{r_{21}r_{32}}+\frac{f_3}{r_{13}r_{32}}\right)\left(f_2+\frac{f_1}{r_{21}}+\frac{f_3}{r_{23}}\right)+f_3\left(\frac{f_1}{r_{13}r_{21}}+\frac{f_2}{r_{23}r_{12}}+\frac{f_3}{r_{13}r_{23}}\right)\left(f_3+\frac{f_1}{r_{31}}+\frac{f_2}{r_{32}}\right)} \tag{5}$$

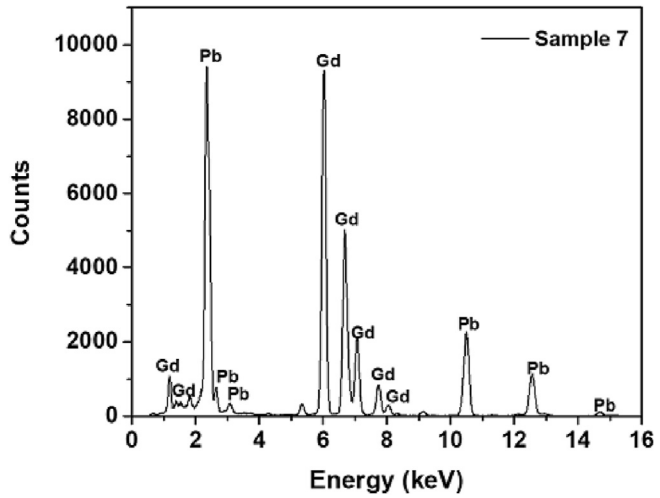

Fig. 5. Typical PIXE spectra of Terpolymer Composition.

2.4.2. Error-in-variables model

Reactivity ratio estimation is a non-linear parameter estimation problem, but its dependent variables have a large error. Parameter estimates obtained by basic linear regression are not accurate. Therefore, EVM is the best method to estimate the multi-component polymerization's reactivity ratios. The basis of the EVM parameter estimation method is first proposed by Reilly and Patino-Leal [37]. Dube et al. [38] and Polic et al. [39] have confirmed that this method is suitable for estimating the reactivity ratios of copolymerization systems. Later, Duever et al. [28] developed an EVM program based on ter-polymerization data to estimate the ternary reactivity ratios, and according to the computational requirements of the ternary problem and the problems in the original form of the AG model, several modifications were made to the EVM program.

In some ter-polymerization works of literature which have been published, there were detailed explanations of the EVM program [40,41], so the details would not be given in this paper.

3. Results and discussion

3.1. The mass attenuation coefficient of metal functional polymers

The shielding rates of the X-ray of different functional polymers were shown in the supporting information (Fig. S1, Fig. S2 and Fig. S3). The MAC of poly (Gd $(MAA)_3$-MMA) and poly (Pb$(MAA)_2$-MMA) for different low-energy X-ray are shown in Fig. 2. As the content of metal functional monomers in the polymer increased, the MAC gradually rose, indicating that the shielding performance of the material against X-ray became better and better. The MAC of poly (Gd $(MAA)_3$-MMA) for X-ray energy of 65 keV was higher than that for energy of 100 keV, while the result of poly (Pb$(MAA)_2$-MMA) was the opposite. It is because that 65 keV was located at the weak absorption energy region of lead.

Fig. 3 illustrates the MAC of poly (Gd $(MAA)_3$-Pb$(MAA)_2$-MMA). The total content of metal functional organic monomers remained constant, and for X-ray with an energy of 65 keV, the MAC increased along with the growth content of Gd, while for 100 keV, the MAC decreased along with the decreasing of the content of Pb. The results of MAC disclosed that to have better shielding performance against X-ray in various low energy ranges, it was better to prepare materials containing both Gd and Pb.

Table 2
Monomer reaction rates estimated by EVM.

r_{12}	r_{21}	r_{13}	r_{31}	r_{23}	r_{32}
0.483	0.004	0.338	2.508	0.255	0.029

*1:Gd$(MAA)_3$, 2:Pb$(MAA)_2$, 3:MMA.

3.2. Comparison of X-ray shielding performance

Fig. 4 illustrates the shielding rate of poly (Gd $(MAA)_3$-MMA) and poly (Pb$(MAA)_2$-MMA) against X-ray with an energy range of 30–100kev. The K shell absorption edges of Gd and Pb are 50.2 and 88 keV respectively. As the X-ray energy increased, the shielding rate of the copolymer gradually decreased. When the X-ray energy reached the absorption edge of the K layer of the metal element, the shielding rate increased sharply and then decreased with the increasing of energy. It is because that in the low energy range, the greater the probability of the photoelectric effect, the better the X-ray shielding performance. The probability of the photoelectric effect is inversely proportional to the third power of energy. But when the energy equaled to the K shell absorption edge of the shielding element, the energy can be completely absorbed by the electrons, which greatly increased the probability of the photoelectric effect. Therefore, the shielding rate increased sharply when the energy reaches the K shell absorption edge of the shielding element [17]. When the energy of X-ray was outside the weak

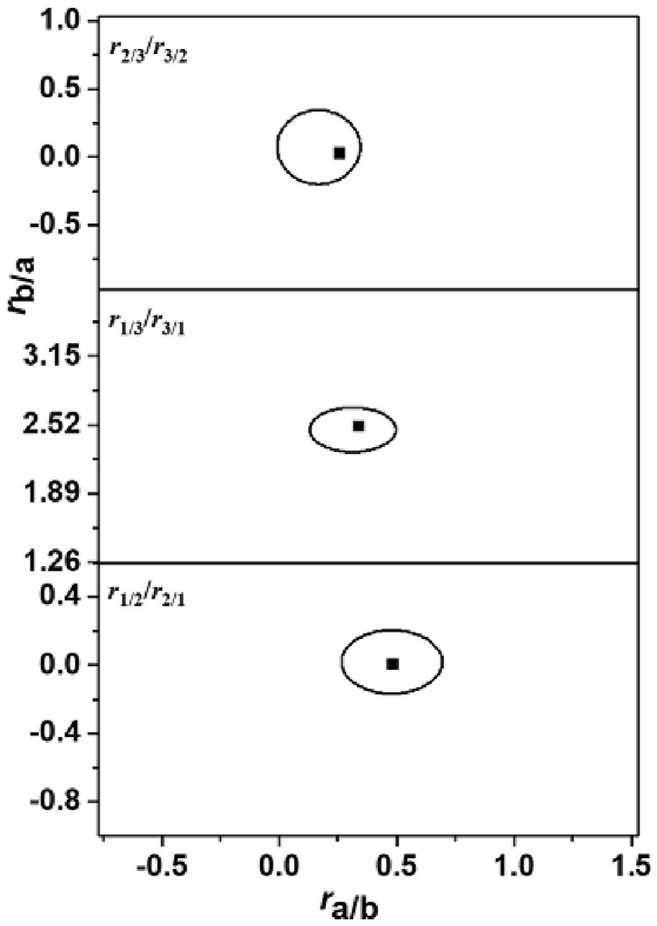

Fig. 6. Ternary reactivity ratios with 95% JCRs for Gd $(MAA)_3$/Pb$(MAA)_2$, Gd $(MAA)_3$/MMA, and Pb$(MAA)_2$/MMA from analysis of random conversion data set with cumulative composition models. *1:Gd $(MAA)_3$, 2:Pb$(MAA)_2$, 3:MMA.

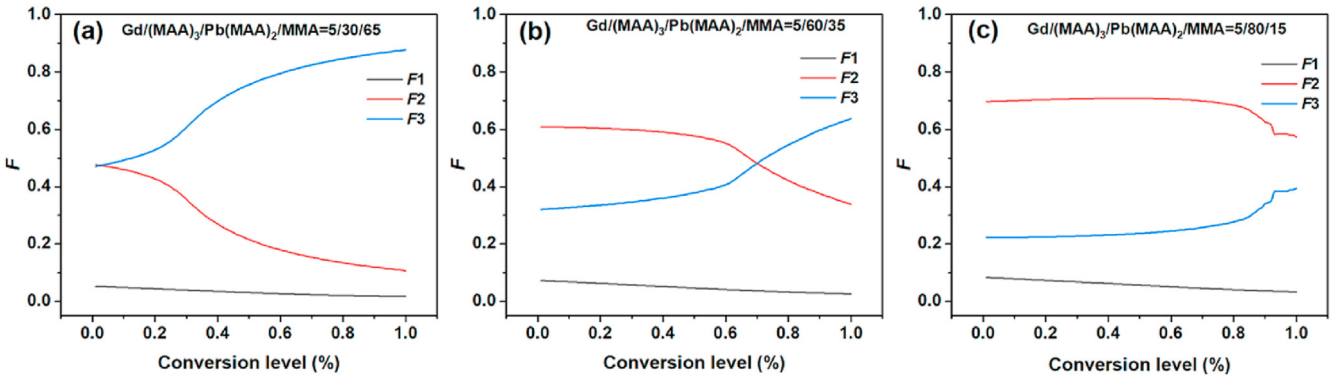

Fig. 7. Prediction cumulative composition of terpolymer under different Gd $(MAA)_3$/$Pb(MAA)_2$/MMA composition.

absorption range of lead, the shielding rate of poly ($Pb(MAA)_2$-MMA) was higher than that of poly (Gd $(MAA)_3$-MMA). This is because that the probability of the photoelectric effect is proportional to the fourth power of the atomic number of the shielding element. In the "lead feeble absorbing area", Gd can compensate for the absorption of X-ray. But Pb is the non-radioactive element with the largest atomic number, considering the shielding effect, Pb should not be completely replaced. Therefore, polymers containing both Gd and Pb could better shield a wide range of low-energy X-ray.

3.3. Ternary reactivity ratios

3.3.1. Terpolymer composition

In the XRD (Fig. S4) and FTIR (Fig. S5) spectra of poly (Gd $(MAA)_3$-$Pb(MAA)_2$-MMA), the characteristic diffraction peaks of $Pb(MAA)_2$ and Gd $(MAA)_3$ were not observed, and no stretching vibration peak of C=C double bond. All of the above phenomena indicated that Gd and Pb elements were chemically bonded into copolymers by ternary polymerization of gadolinium methacrylate (Gd $(MAA)_3$), lead methacrylate ($Pb(MAA)_2$) and methyl methacrylate (MMA). The compositions of the terpolymers could be obtained by the PIXE technique and ash method for elemental analysis. Fig. 5 depicts a typical PIXE spectrum obtained for sample 7. The feed compositions, terpolymer compositions, and mass conversion levels are summarized in Table 1.

3.3.2. Estimation of ternary reactivity ratios through analysis of random conversion data

The estimated reactivity ratio of the three comonomer pairs can be obtained from the comprehensive data. The values of reactivity ratios are given in Table 2. The corresponding 95% JCRs and the specific values between the two reaction rates are shown in Fig. 6. It is seen from the minimum joint confidence area that the result of ternary reactivity ratios estimation was quite accurate.

As function of conversion level and AG recast form, the obtained ternary reactivity ratios can be used to predict the accumulative compositions of terpolymers, as shown in Fig. 7a, b and 7c, which illustrated the model predicted composition of the terpolymer with different monomer feeding compositions. The content of Gd $(MAA)_3$ in the terpolymer decreased slowly along with the increasing of conversion level, while the content of $Pb(MAA)_2$ in the terpolymer firstly remained constant, then decreased sharply as the conversion level gradually increased. The higher the $Pb(MAA)_2$ content in the monomer composition, the abrupt drop point appeared at the higher the conversion level. Therefore, using the prediction of this model, the metal-organic polymer material with uniform composition distribution in the terpolymer could be obtained by controlling the conversion level. For example, in Fig. 7c, when the monomer composition conversion level was not to exceed 80%, the *F* value of each component in the terpolymer remained almost unchanged as the conversion level increased. The terpolymer with uniform composition could be obtained. As a result, the shielding performance was stable and reliable.

4. Conclusion

In this paper, polymers containing both Gd and Pb were prepared by chemically bonding. The shielding performance of metal-containing functional polymers on X-ray was related to the content of shielding elements and the thickness of the material. To achieve higher shielding performance, the content of Gd and Pb should be increased, or increased the thickness of the shielding material. Gd can make up for the lead feeble absorbing area. Therefore, the polymer containing both Gd and Pb could shield X-ray in various energy ranges more effectively. The combination of the DIN method and AG model avoided calculation errors caused by component drift. The EVM program was used to calculate the reaction reactivity ratios of the terpolymer, and the calculation result was accurate and reliable. By calculating the reaction reactivity ratio of the terpolymer (Gd $(MAA)_3$/$Pb(MAA)_2$ and MMA), it was effectively to predict the composition of the components in the terpolymer. The terpolymers with uniform monomer composition could be obtained by controlling the feeding ratio and conversion level. It is hoped that this research can provide a little help for the design and production of more types of X-ray shielding materials in the future.

Declaration of competing interest

The authors declare that they have no known competing financial interests or personal relationships that could have appeared to influence the work reported in this paper.

Acknowledgements

This study was financially supported by the Aviation Industry Joint Fund (No.6141B05080407) and Natural Science Research Project of Guangling College of Yangzhou University (No. ZKZD18004).

Appendix A. Supplementary data

Supplementary data to this article can be found online at https://doi.org/10.1016/j.net.2021.06.021.

References

[1] A. Alhudhaif, K. Polat, O. Karaman, Determination of COVID-19 pneumonia based on generalized convolutional neural network model from chest X-ray images, Expert Syst. Appl. 180 (2021) 115141, 115141.

[2] S. Nambiar, J.T.W. Yeow, Polymer-composite materials for radiation protection, ACS Appl. Mater. Interfaces 4 (11) (2012) 5717–5726.

[3] P.F. Lou, X.B. Teng, Q.X. Jia, Y.Q. Wang, L.Q. Zhang, Preparation and structure of rare earth/thermoplastic polyurethane fiber for X-ray shielding, J. Appl. Polym. Sci. 136 (17) (2019). https://doi:10.1002/app.47435.

[4] L. Liu, L. He, C. Yang, W. Zhang, R.G. Jin, L.Q. Zhang, In situ reaction and radiation protection properties of Gd(AA)(3)/NR composites, Macromol. Rapid Commun. 25 (12) (2004) 1197–1202.

[5] S. Jayakumar, T. Saravanan, J. Philip, Preparation, characterization and X-ray attenuation property of Gd2O3-based nanocomposites, Appl. Nanosci. 7 (8) (2017) 919–931.

[6] M.I. Sayyed, A.A. Ati, M.H.A. Mhareb, K.A. Mahmoud, K.M. Kaky, S.O. Baki, M.A. Mahdi, Novel tellurite glass (60-x)TeO2-10GeO(2)-20ZnO-10BaO–xBi(2)O(3)for radiation shielding, J. Alloys Compd. 844 (2020). https://doi:10.1016/j.jallcom.2020.155668.

[7] P.P. Jiang, J.B. Chen, X.M. Lin, Chinese Pat., 101319025, Jiangnan University, Peop. Rep, China, 2010.

[8] N. Haruo, U. Hiroshi, N. Kunikazu, *Japanese Pat.*, 53063310, Kyowa Gas Chemical Industry Co., Ltd., Japan, 1978.

[9] C.H. Wang, S. Wang, Y.J. Zhang, Z.F. Wang, J.L. Liu, M. Zhang, Self-polymerization and co-polymerization kinetics of gadolinium methacrylate, J. Rare Earths 36 (3) (2018) 298–303.

[10] Y.J. Zhang, X.T. Guo, C.H. Wang, D.F. Wu, M. Zhang, Self-polymerization and co-polymerization kinetics of lead methacrylate, Rare Met. 40 (3) (2021) 736–742.

[11] N. Kazemi, T.A. Duever, A. Penlidis, Demystifying the estimation of reactivity ratios for terpolymerization systems, AIChE J. 60 (5) (2014) 1752–1766.

[12] A. Jukić, M. Rogošić, E. Vidović, Z. Janović, Terpolymerization kinetics of methyl methacrylate or styrene/dodecyl methacrylate/octadecyl methacrylate systems, Polymer International, Poly. Int 56 (1) (2006) 112–120.

[13] A.D. Azzahari, R. Yahya, M.R. Ahmad, M.B. Zubir, New terpolymers from n-butyl acrylate, glycidyl methacrylate and tetrahydrofurfuryl acrylate: synthesis, characterisation and estimation of reactivity ratios. Fibers and Polymers, *Fiber*, Polymja 15 (3) (2014) 437–445.

[14] I. Šoljić, A. Jukić, Z. Janović, Terpolymerization kinetics of N,N-dimethylaminoethyl methacrylate/alkyl methacrylate/styrene systems. Polymer Engineering & Science, Polym. Eng. Sci. 50 (3) (2009) 577–584.

[15] K.A. Mahmoud, M.I. Sayyed, O.L. Tashlykov, Gamma ray shielding characteristics and exposure buildup factor for some natural rocks using MCNP-5 code, Nucl. Eng. Technol. 51 (2019) 1835–1841.

[16] O. Agar, M.I. Sayyed, F. Akman, H.O. Tekin, M.R. Kaçal, An extensive investigation on gamma ray shielding features of Pd/Ag-based alloys, Nucl. Eng. Technol. 51 (3) (2019) 853–859.

[17] Y. Wang, G.K. Wang, T. Hu, S.P. Wen, S. Hu, L. Liu, Enhanced photon shielding efficiency of a flexible and lightweight rare earth/polymer composite: a Monte Carlo simulation study, Nucl. Eng. Technol. 52 (7) (2020) 1565–1570.

[18] J.J.M. Goeij, Nuclear analytical methods in the life sciences, Biol. Trace Elem. Res. 43–45 (1) (1994) 9–17.

[19] S. Srikanth, G.J.N. Raju, Quantitative study of trace elements in coal and coal related ashes using PIXE, J. Geol. Soc. India 94 (5) (2019) 533–537.

[20] W. Maenhaut, Present role of PIXE in atmospheric aerosol research, Nucl. Instrum. Methods B 363 (2015) 86–91.

[21] J. Reyes-Herrera, J. Miranda, O.G. de Lucio, Simultaneous PIXE and XRF elemental analysis of atmospheric aerosols, Microchem. J. 120 (2015) 40–44.

[22] J. Cruz, M. Manso, V. Corregidor, R.J.C. Silva, E. Figueiredo, M.L. Carvalho, L.C. Alves, Surface analysis of corroded XV–XVI century copper coins by μ-XRF and μ-PIXE/μ-EBS self-consistent analysis, Mater. Char. 161 (2020). https://doi:10.1016/j.matchar.2020.110170.

[23] X.F. Li, G.F. Wang, J.H. Chu, L.D. Yu, Charge integration in external PIXE–PIGE for the analysis of aerosol samples, Instrum. Meth. B. 289 (2012) 1–4.

[24] E. Punzón-Quijorna, M. Kelemen, P. Vavpeti, R. Kavalar, S.K. Fokter, Particle induced x-ray emission (PIXE) for elemental tissue imaging in hip modular prosthesis fracture case, Instrum. Meth. B. 462 (2020) 182–186.

[25] A.R. Justino, N. Canha, C. Gamelas, J.T. Coutinho, S.M. Almeida, Contribution of micro-pixe to the characterization of settled dust events in an urban area affected by industrial activities, J. Radioanal. Nucl. Chem. 322 (3) (2019) 1953–1964.

[26] K. Nadeem, J. Hussain, N.U. Haq, A.U. Haq, I. Ahmad, A proton induced X-ray emission (PIXE) analysis of concentration of major/trace and toxic elements in broiler gizzard and flesh of Tehsil Gujar Khan area in Pakistan, Nucl. Eng. Technol. 51 (8) (2019) 2042–2049.

[27] S. Kavlak, A. Güner, Z.M.O. Rzayev, Functional terpolymers containing vinylphosphonic acid: the synthesis and characterization of poly(vinylphosphonic acid-co-styrene-co-maleic anhydride), J. Appl. Polym. Sci. 125 (5) (2012) 3617–3629.

[28] P.G. Sanghvi, N.K. Pokhriyal, S. Devi, Effect of partitioning of monomer on the reactivities of monomers in microemulsion, J. Appl. Polym. Sci. 84 (10) (2002) 1832–1837.

[29] T. Alfrey, G. Goldfinger, The mechanism of copolymerization, The Journal of Chemical Physics, *J. Chem. Phys.* 12 (6) (1944) 205–209.

[30] N. Kazemi, T.A. Duever, A. Penlidis, Demystifying the estimation of reactivity ratios for terpolymerization systems, AIChE J. 60 (5) (2014) 1752–1766.

[31] N. Kazemi, T.A. Duever, A. Penlidis, A powerful estimation scheme with the error-in-variables-model for nonlinear cases: reactivity ratio estimation examples, Comput. Chem. Eng. 48 (2013) 200–208.

[32] A. Scott, N. Kazemi, A. Penlidis, AMPS/AAm/AAc terpolymerization: experimental verification of the EVM framework for ternary reactivity ratio estimation, Processes 5 (4) (2017) 9–24.

[33] M. Riahinezhad, N. Kazemi, N. McManus, A. Penlidis, Effect of ionic strength on the reactivity ratios of acrylamide/acrylic acid (sodium acrylate) copolymerization, J. Appl. Polym. Sci. 131 (20) (2014) 40949.

[34] N. Kazemi, T.A. Duever, A. Penlidis, Reactivity ratio estimation from cumulative copolymer composition Data,*Macromol*, React. Eng. 5 (9–10) (2011) 385–403.

[35] F.K. Yousefi, A. Jannesari, S. Pazokifard, M.R. Saeb, A.J. Scott, A. Penlidis, Reactivity ratio estimation from cumulative copolymer composition Data,-*Macromol*, React. Eng. 13 (4) (2019) 1900014.

[36] I. Skeist, Copolymerization: the composition distribution curve, J. Am. Chem. Soc. 68 (9) (1946) 1781–1784.

[37] P.M. Reilly, H. Patino-Leal, A bayesian study of the error-in-variables model, Technometrics 23 (3) (1981) 221–231.

[38] M. Dube, R.A. Sanayei, A. Penlidis, K.F. O'Driscoll, P.M. Reilly, A microcomputer program for estimation of copolymerization reactivity ratios, J. Polym. Sci., Polym. Chem. Ed. 29 (5) (1991) 703–708.

[39] A.L. Polic, T.A. Duever, A. Penlidis, Case studies and literature review on the estimation of copolymerization reactivity ratios, J. Polym. Sci., Polym. Chem. Ed. 36 (5) (1998) 813–822.

[40] A. Scott, A. Penlidis, Computational package for copolymerization reactivity ratio estimation: improved access to the error-in-variables-model, Processes, Processes 6 (1) (2018) 8.

[41] A.J. Scott, A. Penlidis, Binary vs. ternary reactivity ratios: appropriate estimation procedures with terpolymerization data, Eur. Polym. J. 105 (2018) 442–450.